Probabilistic Robustness Analysis in High Dimensional Space: Application to Semantic Segmentation Network

Navid Hashemi navid.hashemi@vanderbilt.edu
Department of Computer Science, Vanderbilt University, Nashville, TN, USA

Samuel Sasaki samuel.sasaki@vanderbilt.edu
Department of Computer Science, Vanderbilt University, Nashville, TN, USA

Diego Manzanas Lopez diego.manzanas.lopez@vanderbilt.edu
Department of Computer Science, Vanderbilt University, Nashville, TN, USA

Ipek Oguz ipek.oguz@Vanderbilt.edu
Department of Computer Science, Vanderbilt University, Nashville, TN, USA

Meiyi Ma meiyi.ma@vanderbilt.edu
Department of Computer Science, Vanderbilt University, Nashville, TN, USA

Taylor T. Johnson taylor.johnson@vanderbilt.edu
Department of Computer Science, Vanderbilt University, Nashville, TN, USA

Abstract

Semantic segmentation networks (SSNs) play a critical role in domains such as medical imaging, autonomous driving, and environmental monitoring, where safety hinges on reliable model behavior under uncertainty. Yet, existing probabilistic verification approaches struggle to scale with the complexity and dimensionality of modern segmentation tasks, often yielding guarantees that are too conservative to be practical. We introduce a probabilistic verification framework that is both architecture-agnostic and scalable to high-dimensional outputs. Our approach combines sampling-based reachability analysis with conformal inference (CI) to deliver provable guarantees while avoiding the excessive conservatism of prior methods. To counteract CI's limitations in high-dimensional settings, we propose novel strategies that reduce conservatism without compromising rigor. Empirical evaluation on large-scale segmentation models across CamVid, OCTA-500, Lung Segmentation, and Cityscapes demonstrates that our method provides reliable safety guarantees while substantially tightening bounds compared to SOTA. We also provide a toolbox implementing this technique, available on github.[1]

Keywords: Robustness, Semantic Segmentation, Verification, Conformal Inference

1 Introduction

Deep Neural Networks have achieved outstanding success across diverse domains, including image classification, speech recognition, medical diagnosis, and autonomous systems. However, despite their effectiveness, DNNs remain highly sensitive to input perturbations and adversarial examplescarefully crafted modifications that can cause significant changes in model predictions. This vulnerability poses serious risks, particularly in safety-critical applications such as autonomous driving, and medical imaging, where even a single misprediction may lead to catastrophic consequences.

1. https://github.com/Navidhashemicodes/SSN_Reach_CLP_Surrogate

Research on neural network robustness has generally followed two main directions. Falsification-based approaches aim to uncover adversarial examples that expose a models vulnerabilities (Madry et al., 2017; Goodfellow et al., 2014; Kurakin et al., 2016). While effective for identifying potential failure cases, these methods provide no formal guarantees of safety. In contrast, verification-based approaches seek to certify robustness by proving that a network remains reliable under specified input perturbations (Zhou et al., 2024; Lemesle et al., 2024; Wu et al., 2024). Although these techniques offer provable guarantees, they are typically hindered by severe scalability challenges.

Reachability analysisthe task of computing the set of all possible outputs of a system given a bounded input sethas become a central tool for verifying robustness. In the context of neural networks, it captures how input perturbations propagate through the layers and affect the final prediction. However, reachability analysis quickly becomes computationally infeasible for large-scale models or high-dimensional outputs. Semantic segmentation networks (SSNs), which assign a class label to every pixel, present a particularly difficult case due to their extremely high-dimensional output space and complex architectures, often involving components such as transposed convolutions, max-pooling, and dilated convolutions. For such models, traditional reachability-based methods either fail to scale or yield overly conservative guarantees.

To overcome these challenges, probabilistic verification has emerged as a promising direction (Fischer et al., 2021; Anani et al., 2024; Hao et al., 2022; Marzari et al., 2024). Instead of requiring guarantees to hold for every possible perturbation, this approach establishes them with provable probability under a prescribed distribution of input uncertainty. Such methods tend to scale more effectively and yield informative statistical assurances, particularly when exact reachability bounds or Lipschitz estimates are impractical or overly pessimistic. Yet, current probabilistic techniques remain limited: they often cannot capture complex output specifications and struggle to handle the scale of modern semantic segmentation networks. In this paper, we introduce a scalable, architecture-independent probabilistic verification framework with reduced conservatism, specifically designed for semantic segmentation models. Our approach makes no restrictive assumptions on network layers or structure, and is naturally applicable to high-dimensional outputs.

Related Works.

Probabilistic verification of Neural Networks. Neural networks are extremely nonlinear. This poses significant challenges for establishing probabilistic guarantees. Unlike deterministic techniques for verification of neural networks, the probabilistic techniques for classification task does not directly extend to segmentation tasks. A key obstacle arises from the use of the union bound[2], which causes the guarantees to deteriorate rapidly in high-dimensional segmentation settings. A prominent research direction in probabilistic verification is randomized smoothing, first introduced for classifiers Cohen et al. (2019) and later adapted to segmentation models Fischer et al. (2021), with subsequent improvements in Anani et al. (2024); Hao et al. (2022). More recently, conformal inference has also been explored as a way to provide probabilistic guarantees in classification tasks Jeary et al. (2024). In this work, we extend this line of research by applying conformal inference to segmentation task.

2. $\Pr[P_1 \wedge P_2 \wedge \ldots \wedge P_n] \geq 1 - \sum_{i=1}^{n} (1 - \Pr[P_i])$

Although the guarantee formulation may differ, we numerically show that our method can significantly reduce the conservatism compared to existing SOTA on segmentation tasks.

Deterministic Verification of Neural Networks. Deterministic verification of neural networks aims to provide formal guarantees that the networks outputs meet a given specification for all inputs within a prescribed set. This problem has been addressed using several well-established techniques, such as Satisfiability Modulo Theories (SMT) solvers (Duong et al., 2023; Katz et al., 2017; Wu et al., 2024), Mixed Integer Linear Programming (MILP) formulations (Anderson et al., 2020; Cheng et al., 2017; Tjeng et al., 2017), and different types of reachability analysis (Bak et al., 2020; Tran et al., 2020). Many of these methods can be viewed through the general framework of branch-and-bound algorithms (Bunel et al., 2020), which iteratively partition and prune the input domain to either uncover counterexamples or prove correctness. Prominent tools in this area, including α, β-CROWN (Zhou et al., 2024), PyRAT (Lemesle et al., 2024), and Marabou (Wu et al., 2024), have demonstrated strong results in recent VNN-COMP competitions Brix et al. (2024), consistently ranking at the top of evaluation benchmarks. A key component of branch-and-bound approaches is computing tight output bounds for neural networks over constrained input regions. Techniques like interval arithmetic (Cheng et al., 2017; Pulina and Tacchella, 2010) are commonly employed to compute these bounds, influencing both the accuracy and computational efficiency of the verification.

2 Preliminaries

Notations. We write $x \sim \mathcal{X}$ to indicate that the random variable x is drawn from the distribution $\mathcal{X}$, and $x \overset{\mathcal{X}}{\sim} \mathbf{X}$ to indicate that x is sampled from the set $\mathbf{X}$ according to the distribution $\mathcal{X}$. We use bold letters to represent sets and calligraphic letters to denote distributions. Consider a 3-dimensional tensor $x \in \mathbb{R}^{h \times w \times nc}$, which we flatten into a vector. The vectorized form is denoted as $\mathbf{vec}(x) \in \mathbb{R}^{n_0}$, where $n_0 = nc \times w \times h$. The Minkowski sum is denoted by $\oplus$. The ceiling operator $\lceil x \rceil$ denotes the smallest integer greater than or equal to $x \in \mathbb{R}$. A feedforward neural network with input dimension n_0, l hidden layers of sizes $n_1, \ldots, n_l$, and output dimension N, using the ReLU activation function, is denoted as $[n_0, n_1, \ldots, n_l, N](\text{ReLU})$. Her we denote, a ℓ_2 ball with radius $r \in \mathbb{R}^{n_0}$ and center $x \in \mathbb{R}^{n_0}$ with $\mathbf{B}_r(x)$.

Semantic Segmentation Neural Networks A *semantic segmentation neural network* (SSN) is a nonlinear function that assigns a class label to each pixel $x(i, j)$ in a multichannel input image x, producing a target class label $\mathsf{mask}(i, j)$ from a predefined set of classes $\mathbf{L} = \{1, 2, \ldots, L\}$,

$$\mathsf{SSN} : x \in \mathbb{R}^{h \times w \times nc} \mapsto \mathsf{mask} \in \mathbf{L}^{h \times w},$$

where h, w, and nc denote the height, width, and number of channels of the input image, respectively, and $(i, j) \in 1, \ldots, h \times 1, \ldots, w$ are pixel coordinates. In this paper, we denote the logits of SSNs by $y \in \mathbb{R}^{h \times w \times L}$, where the target class label $\mathsf{mask}(i, j)$ is given by $\mathsf{mask}(i, j) = \underset{l \in \mathbf{L}}{\arg\max}\ y(i, j, l)$. Here, we also define the function $f : \mathbb{R}^{n_0} \mapsto \mathbb{R}^n$ as a nonlinear map between the flattened images and the flattened logits. Formally,

$$f : \ \mathbf{vec}(x) \in \mathbb{R}^{n_0} \mapsto \mathbf{vec}(y) \in \mathbb{R}^n, \quad n_0 = h \times w \times nc, \ n = h \times w \times L.$$

Conformal Inference Consider a collection of i.i.d and positive scalar random variables $\mathbf{M} = \{R_1, R_2, \ldots, R_m\}$ sampled from $R \sim \mathcal{D}$, where $R_1 < R_2 < \ldots < R_m$. Given a new draw R_{m+1} from the same distribution and a miscoverage level $\epsilon \in (0, 1)$, conformal inference (CI)(Vovk et al., 2005) constructs a prediction interval $C(R_{m+1}) = [0, d]$ such that $\Pr[\ \ R_{m+1} \in C(R_{m+1})\ \ ] \geq 1 - \epsilon$. In this paper, we refer to these scalar random variables as *nonconformity scores* and we refer to $\mathbf{M}$ as the calibration dataset. To compute the threshold d, we use the empirical distribution of nonconformity scores R_i for $i \in 1, 2, \ldots, m$, and define a rank $\ell := \lceil (m+1)(1-\epsilon) \rceil$. A valid choice for the threshold d is then R_ℓ, the ℓ-th smallest element of the augmented set $R_1, \ldots, R_m, \infty$, as defined in (Tibshirani et al., 2019), which yields the following marginal guarantee:

$$\Pr\left[R_{m+1} \leq R_\ell\right] \geq 1 - \epsilon, \tag{1}$$

where the probability is over the joint randomness of both the calibration and test samples (Tibshirani et al., 2019; Vovk et al., 2005). The test sample R_{m+1} typically refers to an unseen example drawn from the same distribution for which we aim to provide a coverage guarantee. In this paper, we also refer to this sample as the *unseen*, and denote it by R^{unseen}.

Given a sampled calibration dataset, the coverage level $\delta = \Pr[R^{\text{unseen}} \leq R_\ell]$ is itself a random variable following a $\text{Beta}(\ell, m+1-\ell)$ distribution (Angelopoulos and Bates, 2021). The following equations shows the mean value and the variance of the beta distribution in terms of m, ℓ:

$$\mathbf{E}\big[\delta\big] = \frac{\ell}{m+1}, \quad \mathbf{Var}\big[\delta\big] = \frac{\ell(m+1-\ell)}{(m+1)^2(m+2)}, \tag{2}$$

that shows by appropriately tuning m and ℓ, we can significantly reduce the variance $\mathbf{Var}[\delta]$, to avhieve tighter bounds. For instance, when $m = 8000$ and $\ell = 7999$, the variance of the corresponding Beta distribution is 3.123×10^{-8}, which is extremely small.

However, to present this in a completely formal way, we only considers low variance scenarios ($\mathbf{Var}(\delta) \ll 1$) and we also include this source of uncertainty by reformulating this guarantee with a double-step probablistic guarantee. To include this uncertainty, we can utilize the cumulative density function, CDF, of beta distribution- a function known as regularized incomplete beta function- and propose the following guarantee based on the definition of the CDF.

$$\Pr\left[\ \ \Pr\left[\ \ R^{\text{unseen}} \leq R_\ell\ \ \right] > 1 - \epsilon\ \ \right] > 1 - \mathsf{betacdf}_{1-\epsilon}(\ell, m+1-\ell). \tag{3}$$

where $\mathsf{betacdf}_{1-\epsilon}(\ell, m+1-\ell)$ is the regularized incomplete beta function that is characterized by the choice of m and ℓ evaluated at point $\delta_1 = 1 - \epsilon$. The one-step marginal guarantee in (1) holds only when the rank is set to $\ell := \lceil (m+1)(1-\epsilon) \rceil$. However, as shown in Appendix A, a key advantage of the double-step probabilistic guarantee is its flexibility: the strict relationship among m, ℓ, and ϵ can be relaxed. Therefore, in this paper, we focus on the double-step guarantee and do not enforce the constraint $\ell := \lceil (m+1)(1-\epsilon) \rceil$. Instead, we tune m, ℓ, and ϵ such that $\mathsf{betacdf}_{1-\epsilon}(\ell, m+1-\ell)$ becomes negligibly small. Henceforth, for any logical statement $P(\ell, m) \in \{\text{true}, \text{false}\}$, defined over the hyper-parameters $m, \ell \leq m$, we refer to the double-step guarantee,

$$\Pr\left[\ \ \Pr\left[\ \ P(\ell, m)\ \ \right] > 1 - \epsilon\ \ \right] > 1 - \mathsf{betacdf}_{1-\epsilon}(\ell, m+1-\ell)$$

as the $\langle \epsilon, \ell, m \rangle$ guarantee and we say the statement $P(\ell, m)$ satisfies a $\langle \epsilon, \ell, m \rangle$ guarantee. We also refer to ϵ as the miscoverage level, $\delta_1 := 1 - \epsilon$, as the coverage level and $\delta_2 := 1 - \mathsf{betacdf}_{1-\epsilon}(\ell, m+1-\ell)$ as the confidence of guarantee. Appendix B provides a clarifying example on this topic.

Determinitic and Probabilistic Reachability Analysis on Neural Networks Given a neural network $f : \mathbb{R}^{n_0} \to \mathbb{R}^n$ and an input set $\mathbf{I} \subset \mathbb{R}^{n_0}$, *deterministic reachability analysis* aims to construct a set $\mathbf{R}_f(\mathbf{I}) \subset \mathbb{R}^n$ such that

$$x \in \mathbf{I} \quad \Rightarrow \quad f(x) \in \mathbf{R}_f(\mathbf{I}). \tag{4}$$

In contrast, *probabilistic reachability analysis* assumes a distribution $\mathcal{W}$ over the input set $\mathbf{I}$, denoted $x \overset{\mathcal{W}}{\sim} \mathbf{I}$, and for a given miscoverage level ϵ, proposes a set $\mathbf{R}_f^\epsilon(\mathcal{W}) \subset \mathbb{R}^n$ such that

$$x \overset{\mathcal{W}}{\sim} \mathbf{I} \quad \Rightarrow \quad \Pr\left[f(x) \in \mathbf{R}_f^\epsilon(\mathcal{W})\right] \geq 1 - \epsilon. \tag{5}$$

In this paper, we detail how to compute a probabilistic reach set with miscoverage level ϵ, and sampling distribution $x \overset{\mathcal{W}}{\sim} \mathbf{I}$ by constructing a suitable calibration set $\mathbf{M}$ of size m, and selecting an appropriate rank ℓ. Therefore to keep the terminlogies consistent, we reformulate the probabilistic reach set in (5) using the $\langle \epsilon, \ell, m \rangle$ guarantee, and we denote it by $\mathbf{R}_f^\epsilon(\mathcal{W}\,; \ell, m)$, which satisfies

$$x \overset{\mathcal{W}}{\sim} \mathbf{I} \quad \Rightarrow \quad \Pr\left[\Pr\left[f(x) \in \mathbf{R}_f^\epsilon(\mathcal{W}\,; \ell, m)\right] \geq 1 - \epsilon\right] \geq 1 - \mathsf{betacdf}_{1-\epsilon}(\ell, m+1-\ell).$$

Adversarial Examples and Robustness of SSNs An *adversarial attack* on an image involves perturbing the input using a set of noise images $x_1^{\text{noise}}, \ldots, x_r^{\text{noise}}$ and corresponding coefficients $\lambda = [\lambda(1), \ldots, \lambda(r)]^\top$. These perturbations are applied through a parameterized function $\Delta_{\lambda, x^{\text{noise}}}(\cdot)$, generating the adversarial image as:

$$x^{\text{adv}} = \Delta_{\lambda, x^{\text{noise}}}(x) = x + \sum_{i=1}^{r} \lambda(i) x_i^{\text{noise}}. \tag{6}$$

We focus on evaluating the *robustness* of semantic segmentation networks (SSNs) under such adversarial settings, particularly under the unknown, bounded adversarial examples ($x^{\text{adv}} \in \mathbf{I}$) where the coefficients in vector λ are unknown but bounded within specified ranges, i.e., $\lambda \in [\underline{\lambda}, \bar{\lambda}] \subset \mathbb{R}^r$.

A pixel $x(i, j)$ is deemed **attacked** if it faces perturbation. It is also considered **robust** if, for all adversarial examples, the predicted label remains unchanged: $\mathsf{SSN}(\Delta_{\lambda, x^{\text{noise}}}(x))(i, j) = \mathsf{SSN}(x)(i, j)$.

Consider another scenario where there exists perturbations such that the label at (i, j) changes. In this case, the pixel is **non-robust** if for all perturbations we have $\mathsf{SSN}(\Delta_{\lambda, x^{\text{noise}}}(x))(i, j) \neq \mathsf{SSN}(x)(i, j)$. The pixel is also **unknown** if for some perturbations we have $\mathsf{SSN}(\Delta_{\lambda, x^{\text{noise}}}(x))(i, j) = \mathsf{SSN}(x)(i, j)$, and for some other perturbations we have $\mathsf{SSN}(\Delta_{\lambda, x^{\text{noise}}}(x))(i, j) \neq \mathsf{SSN}(x)(i, j)$.

To quantify robustness of SSN we consider two different metrics:

Robustness Value.: The *Robustness Value (RV)* of a network is the percentage of pixels that remain robust under attack: $RV = 100 \times (N_{\text{robust}}/N_{\text{pixels}})$, where $N_{\text{pixels}} = h \times w$.

Problem Formulation Given a SSN, $x \mapsto \mathsf{SSN}(x)$, we address two problems:

Problem 1. Given an input image x, and a desired miscoverage level ϵ, the goal is to determine whether each pixel $x(i,j)$ is robust, non-robust or unknown to a set of adversarial examples $x^{\text{adv}} \in \mathbf{I}$ with strong probabilistic guarantees.

Problem 2. Given K test images $\{x_1, \ldots, x_K\}$, and a set of adversarial examples $\mathbf{I}$, considering a miscoverage level ϵ, compute the average robustness value $\overline{RV}$, with strong probabilistic guarantees.

3 Scaling Probabilistic Reachability Analysis on SSN with Strong Guarantees

Given a specific distribution $x \overset{\mathcal{W}}{\sim} \mathbf{I}$ for sampling inputs x from the input set $\mathbf{I}$, reasoning about the resulting output distribution $y \sim \mathcal{Y}$, is infeasible due to the high degree of nonlinearity in neural networks. As a result, providing probabilistic coverage guarantees over the networks output space becomes a significant challenge. A key advantage of conformal inference is its distributional robustnessit produces valid guarantees that are robust to all family of distributions that can well represent the samples collected in the calibration dataset. This property makes conformal inference particularly well-suited for reachability analysis of neural networks, which are known for producing complex and often intractable output distributions.

However, a major challenge arises when applied to high-dimensional datasets: The scalar elements R in calibration dataset are defined over the outputs $y \sim \mathcal{Y}$ and the space of all possible distributions $\mathcal{Y}$ that can adequately represent the calibration dataset is significantly larger in higher dimensions and thus conformal inference tends to be overly conservative. This poses a significant obstacle when applying CI to semantic segmentation networks (SSNs), which are known for producing extremely high-dimensional outputs. In this paper, we propose a novel learning-based neural network reachability analysis method for SSNs, that leverages deflative principal component analysis (PCA) (Mackey, 2008) to address the dimensionality challenges inherent in conformal inference when applied to provide coverage guarantees on neural network with high dimensional outputs.

In this section, we present our reachability technique in an incremental manner to clearly illustrate both the contributions and the challenges involved in applying conformal inference to SSNs. We begin by introducing a naive baseline approach, then highlight its limitations on high-dimensional spaces. Subsequently, we describe the enhancements we propose to overcome these challenges, culminating in the final version of our reachability algorithm.

3.1 Naive Reachability Technique via Conformal Inference

The first step to find a probabilistic reachset on neural networks with conformal inference (CI) is to generate a calibration dataset $\mathbf{M}$ of size m and a training dataset $\mathbf{T}$ of size t.

Generating train dataset. We sample t different inputs $x_j^{\text{train}}, j = 1, 2, \ldots, t$ from $\mathbf{I}$, with any distribution of interest, $x \overset{\mathcal{W}'}{\sim} \mathbf{I}$, and compute their corresponding outputs $\mathbf{vec}(y_j^{\text{train}}) = f(\mathbf{vec}(x_j^{\text{train}}))$. This gives us the training dataset, $\mathbf{T} = \big\{(x_1^{\text{train}}, y_1^{\text{train}}), (x_2^{\text{train}}, y_2^{\text{train}}), \ldots, (x_t^{\text{train}}, y_t^{\text{train}})\big\}$.

Generating Calibration dataset. We sample the input dataset with m different inputs $x_i^{\text{calib}}, i = 1, 2, \ldots, m$ from the distribution $x \overset{\mathcal{W}}{\sim} \mathbf{I}$ and their corresponding set of outputs $\mathbf{vec}(y_i^{\text{calib}}) = f(\mathbf{vec}(x_i^{\text{calib}})), i = 1, 2, \ldots, m$. This gives us the input/output dataset $\mathbf{IO} = \left\{(x_1^{\text{calib}}, y_1^{\text{calib}}), (x_2^{\text{calib}}, y_2^{\text{calib}}), \ldots, (x_m^{\text{calib}}, y_m^{\text{calib}})\right\}$. We next attempt to use $\mathbf{IO}$ to compute a suitable nonconformity score, $R \in \mathbb{R}_{\geq 0}$. To that end, inspired by recent work on using conformal inference in time-series Cleaveland et al. (2024), we design the nonconformity scores as follows in Equation (7). This design provides us a hyper-rectanglular set. Assuming the output $\mathbf{vec}(y) = [\mathbf{vec}(y)(1), \ldots, \mathbf{vec}(y)(n)] \in \mathbb{R}^n$, we propose, the nonconformity scores R_i^{calib} as,

$$R_i^{\text{calib}} = \max\left(\frac{|\mathbf{vec}(y_i^{\text{calib}})(1) - c(1)|}{\tau_1}, \ldots, \frac{|\mathbf{vec}(y_i^{\text{calib}})(n) - c(n)|}{\tau_n}\right), \quad i = 1, 2, \ldots, m \quad (7)$$

where $c \in \mathbb{R}^n$ is the average of the members in the train dataset $\mathbf{T}$, and for $k = 1, 2, \ldots, n$, the normalization factor τ_k is proposed to normalize the elements of the random vectors $|\mathbf{vec}(y) - c|$ which can also be obtained using the train dataset as,

$$\tau_k := \max\left(\ \tau^*, \max\left(\ \ |\mathbf{vec}(y_1^{\text{train}})(k) - c(k)|, \ \ \ldots, \ \ |\mathbf{vec}(y_t^{\text{train}})(k) - c(k)| \ \ \right)\ \right), \quad (8)$$

where we set $\tau^* = 10^{-5}\left(\sum_{k=1}^{n}\sum_{j=1}^{t}|\mathbf{vec}(y_j^{\text{train}})(k) - c(k)|\right)/nt$, to avoid facing zero as our normalization factor. We then propose the calibration dataset as $\mathbf{M} = \left\{R_1^{\text{calib}}, R_2^{\text{calib}}, \ldots, R_m^{\text{calib}}\right\}$.

The next step is to sort the nonconformity scores in $\mathbf{M}$ based on their magnitude. Without loss of generality let's assume $R_1^{\text{calib}} < R_2^{\text{calib}} < \ldots < R_m^{\text{calib}}$. Given a new draw x^{unseen} from the distribution $x \overset{\mathcal{W}}{\sim} \mathbf{I}$ and the architecture of the neural network, the output $\mathbf{vec}(y^{\text{unseen}}) = f(\mathbf{vec}(x^{\text{unseen}}))$ follows a specific distribution. We call this distribution as $y \sim \mathcal{Y}$. Furthermore given the map we proposed to compute the nonconformity scores, the i.i.d random variables,

$$R^{\text{unseen}} = \max\left(\frac{|\mathbf{vec}(y^{\text{unseen}})(1) - c(1)|}{\tau_1}, \ldots, \frac{|\mathbf{vec}(y^{\text{unseen}})(n) - c(n)|}{\tau_n}\right) \quad (9)$$

adopt another distribution where we call it $R \sim \mathcal{D}$. Here R^{unseen} and the elements $R_1^{\text{calib}}, R_2^{\text{calib}}, \ldots, R_m^{\text{calib}}$ are all sampled from the distribution $\mathcal{D}$. This means that we can apply conformal inference. Therefore, for the new draw R^{unseen}, given a desired rank, $\ell \leq m$ and a desired miscoverage level ϵ, we can propose the following $\langle \epsilon, \ell, m \rangle$ guarantee,

$$\Pr\left[\ \ \Pr[\ \ R^{\text{unseen}} \leq R_\ell^{\text{calib}}\ \ ] > 1 - \epsilon\ \ \right] > 1 - \mathsf{betacdf}_{1-\epsilon}(\ell, m + 1 - \ell).$$

Following the definition in Equation (9), the logical statement $P_1(\ell, m) := [R^{\text{unseen}} \leq R_\ell^{\text{calib}}]$ is logically equivalent to

$$P_2(\ell, m) := \bigwedge_{k=1}^{n}\left[c(k) - \sigma_k \leq \mathbf{vec}(y^{\text{unseen}})(k) \leq c(k) + \sigma_k\right], \quad \text{where } \sigma_k = \tau_k R_\ell^{\text{calib}}, \quad (10)$$

which defines a hyper-rectangular set as the reachset for any unseen output of the neural network generated by $x \overset{\mathcal{W}}{\sim} \mathbf{I}$. Since $P_1(\ell, m)$ satisfies the $\langle \epsilon, \ell, m \rangle$ guarantee, this reachset

also provides the same coverage guarantee on the unseen outputs of the neural network. Appendix C provides a clarifying example on this technique demonstrating that it is effective even on very deep neural networks, offering strong probabilistic guarantees with a reasonable number of required sampling. As the architecture of a deep neural network becomes more complex, the distribution of its output can exhibit increasingly intricate behavior. Conformal inference remains robust to any output distribution that represents well the calibration dataset, allowing it to handle such complexities reliably. However, the tightness of the reachset does not persist when the dimensionality of the networks output increases.

- The first issue is that the naive technique can only produce a hyper-rectangular reachset, that can be a significant source of conservative in high-dimensional spaces.
- The second issue is that the space of distributions $\mathcal{Y}$ that can provide some distribution $\mathcal{D}$ which well represent the calibration dataset is significantly larger in high dimensional space.

3.2 From Hyper-Rectangular Reachsets to Convex Hull Representations

Our approach to constructing a general convex hull as the reachset is based on approximating the original deep neural network f with another computation graph $g : \mathbb{R}^{n_0} \to \mathbb{R}^n$, for which a guaranteed deterministic reachable set can be derived. The model g is generated based on the training dataset $\mathbf{T}$, which implies it is accurate only for inputs x sampled from the set $\mathbf{I}$. The core idea is to utilize its deterministic reachable set, and then **inflate** it to **account for approximation error** between f and its surrogate g, thereby obtaining a probabilistic reachset for the original model f with an $\langle \epsilon, \ell, m \rangle$ guarantee.

Obtaining the surrogate model g serves a **dual** purpose: it not only provides an approximation for f, but also defines the shape of a **convex hull** which when inflated serves as a tighter over-approximation of the probabilistc reachset of f. Once g is computed, this convex shape can be computed as a convex hull. To inflate this surrogate reachset, we follow the procedure outlined in the naive technique (Section 3.1) to generate a hyper-rectangle that bounds the prediction error with a provable $\langle \epsilon, \ell, m \rangle$ guarantee. In other words, we define $q(\mathbf{vec}(x)) = f(\mathbf{vec}(x)) - g(\mathbf{vec}(x))$ and apply the naive technique on $q(\mathbf{vec}(x))$ to compute its hyper-rectangular reachset with $\langle \epsilon, \ell, m \rangle$ guarantee. We refer to this hyper-rectangle as *inflating set*.

In conclusion, if we denote the deterministic reachset of surrogate model as the starset $\mathcal{R}_g(\mathbf{I})$,

$$x \in \mathbf{I} \quad \Rightarrow \quad g(\mathbf{vec}(x)) \in \mathcal{R}_g(\mathbf{I})$$

and for some hyper-parameters (ℓ, m) and distribution $x \overset{\mathcal{W}}{\sim} \mathbf{I}$, the $\langle \epsilon, \ell, m \rangle$ guaranteed probabilistic reachset for prediction errors by $\mathcal{R}_q^\epsilon(\mathcal{W};\ \ell, m)$,

$$x \overset{\mathcal{W}}{\sim} \mathbf{I} \ \Rightarrow\ \Pr\big[\ \Pr[\ \ q(\mathbf{vec}(x)) \in \mathcal{R}_q^\epsilon(\mathcal{W};\ \ell, m)\ ] > 1-\epsilon\ \big] > 1 - \mathsf{betacdf}_{1-\epsilon}(\ell, m+1-\ell),$$

then the probabilistic reachset of the model f with the same $\langle \epsilon, \ell, m \rangle$ guarantee is obtainable by $\mathcal{R}_f^\epsilon(\mathcal{W}; \ell, m) = \mathcal{R}_g(\mathbf{I}) \oplus \mathcal{R}_q^\epsilon(\mathcal{W};\ \ell, m)$, where $\oplus$ denotes the Minkowski sum,

$$x \overset{\mathcal{W}}{\sim} \mathbf{I} \quad \Rightarrow \quad \Pr\big[\ \Pr[\ \ f(\mathbf{vec}(x)) \in \mathcal{R}_f^\epsilon(\mathcal{W}; \ell, m)\ \ ] > 1-\epsilon\ \ \big] > 1 - \mathsf{betacdf}_{1-\epsilon}(\ell, m+1-\ell).$$

Algorithm 1: Learning Based Principal Component Analysis through Deflation Algorithm

Initialize z_1 , z_2, ..., z_t $\leftarrow$ $\mathbf{vec}(y_1^{\text{train}})$, $\mathbf{vec}(y_2^{\text{train}})$, ..., $\mathbf{vec}(y_t^{\text{train}})$, $A \leftarrow$ [ ]
for index $= 0, 1, \ldots N-1$ **do**
  // Train the principal direction using stochastic gradient ascent
  $\vec{a}_{\text{index}} \leftarrow \arg\max_{\vec{a}} \left[\mathcal{J} := \frac{1}{t}\sum_{j=1}^{t} \vec{a}^\top z_j z_j^\top \vec{a}\right], \quad \mathbf{s.t.} \quad \|\vec{a}\|_2 = 1$
  A.**append**$(\vec{a}_{\text{index}})$ // collect the principal direction in A
  // Update the dataset by component removal along principal direction.
  $z_1, z_2, \ldots, z_t \leftarrow z_1 - (\vec{a}_{\text{index}}^\top z_1)\vec{a}_{\text{index}}, z_2 - (\vec{a}_{\text{index}}^\top z_2)\vec{a}_{\text{index}}, \ldots, z_t - (\vec{a}_{\text{index}}^\top z_t)\vec{a}_{\text{index}}$
end

This technique offers two key improvements over the naive approach presented in Section 3.1:

- The reachset is no longer constrained to a hyper-rectangle, eliminating the first source of conservatism inherent in the naive method.
- The calibration dataset is now defined using prediction errors rather than the networks raw outputs. Since prediction errors are typically of much smaller magnitude than the outputs of model f, this significantly reduces the conservatism of conformal inference in high-dimensional spaces. This implies that a useful surrogate model must maintain an acceptable level of fidelity.

To obtain a surrogate model g with high fidelity while ensuring a deterministic reachable set, we propose using the convex hull **CH** over the training outputs y_j^{train}, $j = 1, \ldots, t$,

$$\mathbf{CH} = \sum_{j=1}^{t} \alpha_j \mathbf{vec}(y_j^{\text{train}}), \qquad \mathbf{s.t.} \quad \sum_{j=1}^{t} \alpha_j = 1, \quad \alpha_1, \cdots, \alpha_t > 0$$

and then incorporating a **clipping block** (see Appendix D) that projects the outputs of f for any unseen image x^{unseen}, into this convex hull. Denoting the clipping block with **CLP** we propose the surrogate model as: $g(\mathbf{vec}(x)) = \mathbf{CLP}(f(\mathbf{vec}(x)))$, that makes certain $\mathbf{R}_g(\mathbf{I}) = \mathbf{CH}$.

Despite the improvements introduced in this section, reachability analysis remains unscalable in high-dimensional settings. The fundamental difficulty lies in the fact that projecting $\mathbf{vec}(y^{\text{unseen}})$ on **CH** does not scale well with the dimensionality of the output space. To mitigate this, we incorporate an scalable version of Principal Component Analysis (PCA), known as defelation algorithm, before clipping, a technique known to be effective for handling PCA in high-dimensional spaces. Therefore, the error $q(x)$ primarily arises from the inclusion of PCA and clipping block.

3.3 Surrogate Model for SSNs via Principal Component Analysis

In this section, we present our methodologies to mitigate the dimensionality challenges to provide the surrogate model, and present our technique for the robustness analysis of SSNs.

In our robustness analysis of SSNs, as indicated by equation (6), adversarial perturbations are confined to an r-dimensional subspace of the input space. Thus, we reformulate the surrogate as,

$$g'(\lambda) = g(\ \mathbf{vec}(\ x + \sum_{i=1}^{r} \lambda(i) x^{\text{noise}}\ )\ ) = g(\mathbf{vec}(x^{\text{adv}})) \quad \text{and} \quad \lambda \in [\underline{\lambda}, \overline{\lambda}] \subset \mathbb{R}^r,$$

and also the deterministic reachset $\mathbf{R}_g(\mathbf{I})$ based on the vector λ as $\mathbf{R}_{g'}([\underline{\lambda}, \overline{\lambda}]) = \mathbf{R}_g(\mathbf{I}) = \mathbf{CH}$.

High-Dimensionality of Output Space. To address this challenge, we firt reduce the dimensionality of the logits i.e., for a choice of $N \ll n$, and then generate the convex hull to be used in the clipping process. Let's sample training images x_j^{train}, for $j = 1, \ldots, t$, from the adversarial set $\mathbf{I}$, using sampling the coefficient vectors λ_j^{train} form $[\underline{\lambda}, \overline{\lambda}]$. Then the corresponding logits $\mathbf{vec}(y_j^{\text{train}})$ form a point cloud in $\mathbb{R}^n$. This stage aims to train the top N principal directions of cloud, which are stored as columns of the matrix $A = [\vec{a}_0,\ \vec{a}_1,\ \ldots,\ \vec{a}_{N-1}] \in \mathbb{R}^{n \times N}$.

We utilize this matrix to represent the high dimensional logits y_j^{train} with a lower dimentional representative $v_j \in \mathbb{R}^N$ where $v_j = A^\top \mathbf{vec}(y_j^{\text{train}})$. Principal Component Analysis is a technique to reduce the dimensionalty, but it does not scale to high dimensional spaces. To address this issue, deflation algorithms have been proposed (see Algorithm 1) that compute principal components iteratively, in order of significance (Mackey, 2008). At each iteration, once the most dominant principal component is identified, the dataset is projected onto the orthogonal complement of that directioneffectively removing its contributionbefore computing the next principal direction.

In this paper, we adopt a learning based deflation algorithm that is presented in Algorithm 1. In this algorithm we set the components of the principal direction as trainable parameters and maximize the variance of the dataset in the direction of this vector. At each iteration of this algorithm, the optimization to train the principal direction have one global maxima one global minima and $n-2$ saddle points, which n is the dimension of logits $\mathbf{vec}(y_j^{\text{train}})$ Mackey (2008). Therefore, although the training operates in a high-dimensional space, convergence to global maxima is guaranteed.

Next we generate the convex hull over the cloud of point of the low dimensional representatives of logit $v_j, j = 1, \ldots, t$ and then apply the clipping block. Thus, for any unseen λ we define,

$$g'(\lambda^{\text{unseen}}) = g(x^{\text{adv}}) = A\ \mathbf{CLP}(A^\top f(\mathbf{vec}(\ x + \sum_{i=1}^{r} \lambda^{\text{unseen}}(i) x^{\text{noise}}\ )))$$

In conclusion we present the surrogate model for f as $g(x^{\text{adv}})$ which is a scalable choice for SSNs.

Detecting Robust, Nonrobust and Unknown Pixels with Strong Probabilistic Guarantees Once the reachset over the SSN logits $y \in \mathbb{R}^n$ is constructed as a starset, we project it onto each logit component. This allows us to determine the range of values for each class label $l \in \mathbf{L}$ at every pixel location $(i, j) \in \{1, \ldots, h\} \times \{1, \ldots, w\}$. Consequently, each pixel (i, j) is associated with L logit intervals, one for each class. Let $l^* \in \mathbf{L}$ denote the

Table 1: Model details and probabilistic guarantees. Given hyperparameters ℓ, m, and coverage $\delta_1 = 1 - \epsilon$, the confidence δ_2 is computed for each experiment. The reported verification runtime is averaged over all experiments run on a model. One important point is, our verification runtime depends mainly on inference time, and hyperparameters (ℓ, m), and is only slightly sensitive to perturbation magnitude and dimension (e, r). For per-experiment runtimes, see Figure 5 in Appendix E.

Dataset name	Model name	Input dimension	Output dimension	Number of Parameters	$(m, m-\ell)$	coverage δ_1	confidence δ_2	Average runtime (method)
Lung Segmentation	UNet1	512×512×1	512×512×1	14,779,841	(8e3, 1)	0.999	0.997	5.6 min (Surrogate)
OCTA-500	UNet2	304×304×1	304×304×1	5,478,785	(8e3, 1)	0.999	0.997	9.8 min (Surrogate)
CamVid	BiSeNet	720×960×3	720×960×12	12,511,084	(8e3, 1)	0.999	0.997	18.3 min (Surrogate)
Cityscapes (Appendix E)	HRNetV2	1024×2048×3	256×512×19	65,859,379	(921, 1)	0.99	0.997	3.5 min (Naive)

class whose logit interval has the highest lower bound at pixel (i, j). If this lower bound is not strictly greater than the upper bounds of all other classes' intervals, the pixel is labeled as *unknown* as it can obtain more than one labels under UBAA. In case it is greater, then if $l^* = \mathsf{SSN}(x)(i, j)$, the prediction at that pixel is labeled as *robust* and if $l^* \neq \mathsf{SSN}(x)(i, j)$, it is labeled as *non-robust*. The Algorithm 2 explains this procedure in detail.

4 Experiments

In our numerical evaluation, we pose three different research questions and address each of them using numerical results. The main one is available in this section and the rest of them are in Appendix E. We utilized a Linux machine, with 48 GB of GPU memory, 512 GB of RAM, and 112 CPUs.

Algorithm 2: Detection of the pixel status

Input: $\mathbf{I}$, x, f, $\mathcal{W}$, ϵ, Hyper-parameters(ℓ, m)
Output: The status of pixels

```
// Project the Starset
```
$[\underline{y}, \overline{y}] \leftarrow \mathcal{R}^{\epsilon}_{f}(\mathcal{W}; \ell, m)$
foreach $(i, j) \in \{1{:}h\} \times \{1{:}w\}$ **do**
  $l^* \leftarrow \arg\max_l \underline{y}(i, j, l)$
  if $\underline{y}(i, j, l^*) \leq \max_{l \neq l^*} \overline{y}(i, j, l)$ **then**
    Label pixel (i, j) as `unknown`
  end
  else if $l^* = \mathsf{SSN}(x)(i, j)$ **then**
    Label pixel (i, j) as `robust`
  end
  else
    Label pixel (i, j) as `nonrobust`
  end
end
return *Pixel-wise labeling*

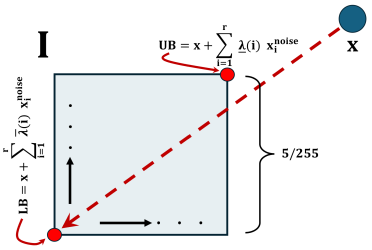

Figure 1: Illustrates the perturbation set $\mathbf{I}$ corresponding to an r-dimensional darkening adversary on image x. This set is made by independent perturbations on all nc channels in r' different pixels ($r = nc \times r'$), each with R,G, and B intensities greater than 150/255. The lower bound **LB** represents the maximum darkening (channel intensities set to zero), while the upper bound **UB** corresponds to minimum darkening.

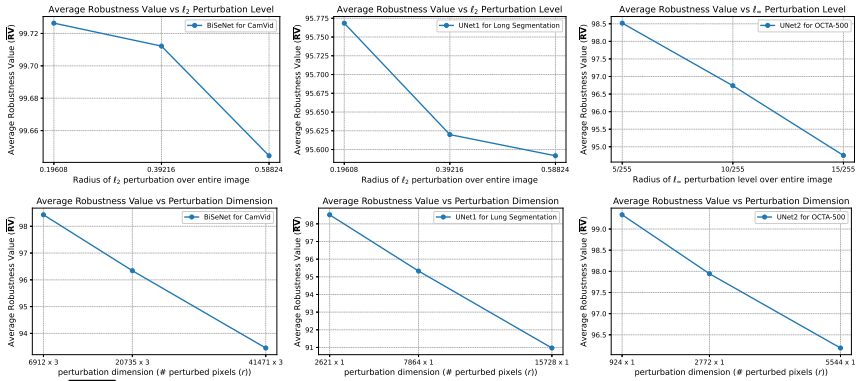

Figure 2: Shows $\overline{\mathbf{RV}}$ versus perturbation level and perturbation dimension. In the top row, we perturbed the entire image with ℓ_2 perturbation for CamVid and Lung Segmentation and ℓ_∞ for OCTA-500. In the bottom row, we consider darkening adversary with $e = 5/255$ and we increase the dimension of perturbation. Robustness is averaged over 200 test images
.

RQ1: How does the technique scale with model size, number of perturbed pixels, and perturbation level? How does output high dimensionality, and the irregularity in output distribution of large and complex NNs make our guarantees overly conservative? To assess scalability, we test our verification method on high-dimensional datasets (e.g., Lung Segmentation (Jaeger et al., 2014; Candemir et al., 2014), OCTA-500 (Li et al., 2019), CamVid (Brostow et al., 2009)) using large pre-trained models. We evaluate performance on a subset of 200 test images across varying perturbation dimensions and magnitudes, with results shown in Figure 2. Model details and probabilistic guarantees are summarized in Table 1, where we show the following $\langle \epsilon, \ell, m \rangle$ guarantee:

$$\Pr\left[\Pr\left[\mathsf{P}\right] \geq \delta_1\right] \geq \delta_2, \quad \text{where } \mathsf{P} := \text{“} \left\{ \begin{array}{l} \text{Given an image } x\text{, the perturbation magnitude and dimension } e, r, \\ \text{the computed robustness value } \mathbf{RV} \text{ from our technique is valid.} \end{array} \right\} \text{”}$$

In these experiments, we studied an r-dimensional darkening adversary (see Figure 1), where r' pixels in an image x with intensity above 150/255 in all channels are randomly selected for perturbation ($r = nc \times r'$). Each direction x_i^{noise} corresponds to darkening a channel of one such pixels, and x^{adv} is parameterized by an r-dimensional coefficient vector $\lambda \in [\underline{\lambda}, \overline{\lambda}]$. Here, $\overline{\lambda}$ induces full darkening (intensity zero), while $\underline{\lambda}$ applies partial darkening. This bound defines the perturbation space $x^{\text{adv}} \in \mathbf{I}$. We also present a demo for the status of all pixels in the segmentation mask in Figures 6,7 and 8.

To assess the conservatism, we examine the projection bounds $[\underline{y}, \overline{y}]$ introduced in Algorithm 2. Specifically, we sample 10^6 adversarial examples from $x^{\text{adv}} \overset{\mathcal{W}}{\sim} \mathbf{I}$ and use them to report:

- Empirical miscoverage $\hat{\epsilon}$, that is the percentage of events, where $f(\mathbf{vec}(x^{\text{adv}})) \notin [\underline{y}, \overline{y}]$.
- Empirical bound $[\underline{\hat{y}}, \overline{\hat{y}}]$, via component-wise minima/maxima of $f(\mathbf{vec}(x^{\text{adv}}))$ across samples.

The degree of conservatism can be assessed by comparing $[\underline{\hat{y}}, \overline{\hat{y}}]$ with $[\underline{y}, \overline{y}]$. To measure this, we compute $\mathsf{bound\_ratio} = \sum_{k=1}^{h \times w \times L} (\overline{\hat{y}}(k) - \underline{\hat{y}}(k)) / \sum_{k=1}^{h \times w \times L} (\overline{y}(k) - \underline{y}(k))$ and due to the

high cost of 10^6 inferences on the models, we only perform the conservatism analysis on one specific case with BiSeNet from Figure 2, Table 2 in Appendix E details the numerical results.

5 Conclusion

Our probabilistic verification method is both scalable and data-efficient. While it does not offer deterministic guarantees, it can provide meaningful assurances in regions where existing deterministic tools are not applicable due to computational challenges. In this paper, we also demonstrated this capability through a series of numerical experiments.

References

A. Anani, T. Lorenz, B. Schiele, and M. Fritz. Adaptive hierarchical certification for segmentation using randomized smoothing. *arXiv preprint arXiv:2402.08400*, 2024.

R. Anderson, J. Huchette, W. Ma, C. Tjandraatmadja, and J. P. Vielma. Strong mixed-integer programming formulations for trained neural networks. *Mathematical Programming*, 183(1):3–39, 2020.

A. N. Angelopoulos and S. Bates. A gentle introduction to conformal prediction and distribution-free uncertainty quantification. *arXiv preprint arXiv:2107.07511*, 2021.

S. Bak, H.-D. Tran, K. Hobbs, and T. T. Johnson. Improved geometric path enumeration for verifying relu neural networks. In *Computer Aided Verification: 32nd International Conference, CAV 2020, Los Angeles, CA, USA, July 21–24, 2020, Proceedings, Part I 32*, pages 66–96. Springer, 2020.

C. B. Barber, D. P. Dobkin, and H. Huhdanpaa. The quickhull algorithm for convex hulls. *ACM Transactions on Mathematical Software (TOMS)*, 22(4):469–483, 1996.

C. Brix, S. Bak, T. T. Johnson, and H. Wu. The fifth international verification of neural networks competition (vnn-comp 2024): Summary and results. *arXiv preprint arXiv:2412.19985*, 2024.

G. J. Brostow, J. Fauqueur, and R. Cipolla. Semantic object classes in video: A high-definition ground truth database. *Pattern Recognition Letters*, 30(2):88–97, 2009. ISSN 0167-8655. doi: https://doi.org/10.1016/j.patrec.2008.04.005. URL `https://www.sciencedirect.com/science/article/pii/S0167865508001220`. Video-based Object and Event Analysis.

R. Bunel, J. Lu, I. Turkaslan, P. H. Torr, P. Kohli, and M. P. Kumar. Branch and bound for piecewise linear neural network verification. *Journal of Machine Learning Research*, 21(42):1–39, 2020.

S. Candemir, S. Jaeger, K. Palaniappan, J. P. Musco, R. K. Singh, Zhiyun Xue, A. Karargyris, S. Antani, G. Thoma, and C. J. McDonald. Lung segmentation in chest radiographs using anatomical atlases with nonrigid registration. *IEEE Trans. Med. Imaging*, 33(2): 577–590, Feb. 2014.

M. Casadio, T. Dinkar, E. Komendantskaya, L. Arnaboldi, M. L. Daggitt, O. Isac, G. Katz, V. Rieser, and O. Lemon. Nlp verification: Towards a general methodology for certifying robustness.(2025). *arXiv preprint cs.CL/2403.10144*, 2025.

B. CE. Pubblicazioni del r instituto superiore di scienze economiche e commerciali di firenze. *Teoria statistica delle classi ecalcolo delle probabilità*, 8:3–62, 1936.

C.-H. Cheng, G. Nührenberg, and H. Ruess. Maximum resilience of artificial neural networks. In *Automated Technology for Verification and Analysis: 15th International Symposium, ATVA 2017, Pune, India, October 3–6, 2017, Proceedings 15*, pages 251–268. Springer, 2017.

K. L. Clarkson. Applications of random sampling in computational geometry, ii. In *Proceedings of the fourth annual symposium on Computational geometry*, pages 1–11, 1988.

M. Cleaveland, I. Lee, G. J. Pappas, and L. Lindemann. Conformal prediction regions for time series using linear complementarity programming. In *Proceedings of the AAAI Conference on Artificial Intelligence*, volume 38, pages 20984–20992, 2024.

J. Cohen, E. Rosenfeld, and Z. Kolter. Certified adversarial robustness via randomized smoothing. In *international conference on machine learning*, pages 1310–1320. PMLR, 2019.

M. Cordts, M. Omran, S. Ramos, T. Rehfeld, M. Enzweiler, R. Benenson, U. Franke, S. Roth, and B. Schiele. The cityscapes dataset for semantic urban scene understanding. In *Proceedings of the IEEE conference on computer vision and pattern recognition*, pages 3213–3223, 2016.

H. A. David and H. N. Nagaraja. *Order statistics*. John Wiley & Sons, 2004.

H. Duong, T. Nguyen, and M. Dwyer. A dpll (t) framework for verifying deep neural networks. *arXiv preprint arXiv:2307.10266*, 2023.

R. A. Dwyer. *Average-case analysis of algorithms for convex hulls and Voronoi diagrams*. Carnegie Mellon University, 1988.

M. Fiacchini and T. Alamo. Probabilistic reachable and invariant sets for linear systems with correlated disturbance. *Automatica*, 132:109808, 2021.

M. Fischer, M. Baader, and M. Vechev. Scalable certified segmentation via randomized smoothing. In *International Conference on Machine Learning*, pages 3340–3351. PMLR, 2021.

I. J. Goodfellow, J. Shlens, and C. Szegedy. Explaining and harnessing adversarial examples. *arXiv preprint arXiv:1412.6572*, 2014.

Z. Hao, C. Ying, Y. Dong, H. Su, J. Song, and J. Zhu. Gsmooth: Certified robustness against semantic transformations via generalized randomized smoothing. In *International Conference on Machine Learning*, pages 8465–8483. PMLR, 2022.

S. Holm. A simple sequentially rejective multiple test procedure. *Scandinavian journal of statistics*, pages 65–70, 1979.

S. Jaeger, A. Karargyris, S. Candemir, L. Folio, J. Siegelman, F. Callaghan, Zhiyun Xue, K. Palaniappan, R. K. Singh, S. Antani, G. Thoma, Yi-Xiang Wang, Pu-Xuan Lu, and C. J. McDonald. Automatic tuberculosis screening using chest radiographs. *IEEE Trans. Med. Imaging*, 33(2):233–245, Feb. 2014.

L. Jeary, T. Kuipers, M. Hosseini, and N. Paoletti. Verifiably robust conformal prediction. *Advances in Neural Information Processing Systems*, 37:4295–4314, 2024.

Y. Jia, S. Zhang, H. Wang, Y. Wen, L. Fu, H. Long, X. Wang, and C. Zhou. Investigating the geometric structure of neural activation spaces with convex hull approximations. *Neurocomputing*, 499:93–105, 2022.

G. Katz, C. Barrett, D. L. Dill, K. Julian, and M. J. Kochenderfer. Reluplex: An efficient smt solver for verifying deep neural networks. In *Computer Aided Verification: 29th International Conference, CAV 2017, Heidelberg, Germany, July 24-28, 2017, Proceedings, Part I 30*, pages 97–117. Springer, 2017.

A. Kurakin, I. Goodfellow, and S. Bengio. Adversarial machine learning at scale. *arXiv preprint arXiv:1611.01236*, 2016.

A. Lemesle, J. Lehmann, and T. L. Gall. Neural network verification with pyrat. *arXiv preprint arXiv:2410.23903*, 2024.

M. Li, S. Yuan, and Q. Chen. Octa-500, 2019. URL `https://dx.doi.org/10.1016/j.media.2024.103092`.

L. Mackey. Deflation methods for sparse pca. *Advances in neural information processing systems*, 21, 2008.

A. Madry, A. Makelov, L. Schmidt, D. Tsipras, and A. Vladu. Towards deep learning models resistant to adversarial attacks. *arXiv preprint arXiv:1706.06083*, 2017.

L. Marzari, D. Corsi, E. Marchesini, A. Farinelli, and F. Cicalese. Enumerating safe regions in deep neural networks with provable probabilistic guarantees. In *Proceedings of the AAAI Conference on Artificial Intelligence*, volume 38, pages 21387–21394, 2024.

L. Pulina and A. Tacchella. An abstraction-refinement approach to verification of artificial neural networks. In *Computer Aided Verification: 22nd International Conference, CAV 2010, Edinburgh, UK, July 15-19, 2010. Proceedings 22*, pages 243–257. Springer, 2010.

H. Sartipizadeh and T. L. Vincent. Computing the approximate convex hull in high dimensions. *arXiv preprint arXiv:1603.04422*, 2016.

R. J. Tibshirani, R. Foygel Barber, E. Candes, and A. Ramdas. Conformal prediction under covariate shift. *Advances in neural information processing systems*, 32, 2019.

V. Tjeng, K. Xiao, and R. Tedrake. Evaluating robustness of neural networks with mixed integer programming. *arXiv preprint arXiv:1711.07356*, 2017.

H.-D. Tran, S. Bak, W. Xiang, and T. T. Johnson. Verification of deep convolutional neural networks using imagestars. In *International conference on computer aided verification*, pages 18–42. Springer, 2020.

H.-D. Tran, N. Pal, P. Musau, D. M. Lopez, N. Hamilton, X. Yang, S. Bak, and T. T. Johnson. Robustness verification of semantic segmentation neural networks using relaxed reachability. In *International conference on computer aided verification*, pages 263–286. Springer, 2021.

V. Vovk, A. Gammerman, and G. Shafer. *Algorithmic learning in a random world*, volume 29. Springer, 2005.

J. Wang, K. Sun, T. Cheng, B. Jiang, C. Deng, Y. Zhao, D. Liu, Y. Mu, M. Tan, X. Wang, et al. Deep high-resolution representation learning for visual recognition. *IEEE transactions on pattern analysis and machine intelligence*, 43(10):3349–3364, 2020.

H. Wu, O. Isac, A. Zeljić, T. Tagomori, M. Daggitt, W. Kokke, I. Refaeli, G. Amir, K. Julian, S. Bassan, et al. Marabou 2.0: a versatile formal analyzer of neural networks. In *International Conference on Computer Aided Verification*, pages 249–264. Springer, 2024.

D. Zhou, C. Brix, G. A. Hanasusanto, and H. Zhang. Scalable neural network verification with branch-and-bound inferred cutting planes. *arXiv preprint arXiv:2501.00200*, 2024.

Appendix A. Double-Step Probabilistic Guarantee

The necessary steps to establish the two-sided probabilistic guarantee, along with the flexibility in choosing the dataset size m, rank ℓ, and failure probability ϵ, begin with the theory of order statistics David and Nagaraja (2004). This flexibility means that the double-step probability constraint remains valid regardless of the particular values chosen for m, $\ell \leq m$, and $\epsilon \in [0, 1]$. The following lemma introduces the concept of order statistics.

Lemma 1 (From David and Nagaraja (2004)) *Consider m independent and identically distributed (i.i.d.), real-valued data points $x \in [0, 1]$ drawn from uniform distribution $x \sim \mathcal{U}$. Suppose we sort them in ascending order and denote the ℓ^{th} smallest number by x_ℓ,(i.e., we have $x_1 < x_2 < \ldots < x_m$). Let $\mathbf{Beta}(\alpha, \beta)$ denote the Beta distribution[3]. Then the uniform random variable at rank ℓ follows:*

$$x_\ell \sim \mathbf{Beta}(\ell, m + 1 - \ell)$$

In the context of conformal inference Lemma 1, has been extended from a uniform and domain-bounded distribution to a general distribution as follows:

3. The Beta distribution is a family of continuous probability distributions defined on the interval $0 \leq x \leq 1$ with shape parameters α and β, and with probability density function $f(x; \alpha, \beta) = \frac{x^{\alpha-1}(1-x)^{\beta-1}}{B(\alpha,\beta)}$, where the constant $B(\alpha, \beta) = \frac{\Gamma(\alpha)\Gamma(\beta)}{\Gamma(\alpha+\beta)}$ and $\Gamma(z) = \int_0^\infty t^{z-1}e^{-t}\mathbf{d}t$ is the Gamma function.

Lemma 2 (From Vovk et al. (2005)) *Consider m independent and identically distributed (i.i.d.), real-valued data points R drawn from some distribution $R \sim \mathcal{D}$. Suppose we sort them in ascending order and denote the ℓ^{th} smallest number by R_ℓ, (i.e., we have $R_1 < R_2 < \ldots < R_m$). Let $\mathbf{Beta}(\alpha, \beta)$ denote the Beta distribution. Then, for an arbitrary R_{m+1} drawn from the same distribution $\mathcal{D}$, the following holds:*

$$\Pr\left[R_{m+1} < R_\ell\right] \sim \mathbf{Beta}(\ell, m+1-\ell), \quad 1 \leq \ell \leq m. \tag{11}$$

This result is motivated by two key observations: (1) for a continuous distribution $R \sim \mathcal{D}$, the cumulative probability $\Pr[R \leq r]$ is uniformly distributed on $[0, 1]$, and (2) sorting the samples $R_1 < R_2 < \ldots < R_m$ implies that the corresponding cumulative probabilities $\Pr[R \leq R_\ell]$ are also ordered, i.e., $\Pr[R \leq R_1] < \Pr[R \leq R_2] < \ldots < \Pr[R \leq R_m]$. These observations implies that for all $\ell = 0, 1, 2, \ldots, m$, the random variable $\delta := \Pr[R \leq R_\ell]$ satisfies the conditions outlined in Lemma 1.

In simple terms, this means that while a fixed dataset $R_1, R_2, \ldots, R_m$ is not sufficient to determine the exact value of $\delta = \Pr[R < R_\ell]$, we can infer that the value of δ must follow a Beta distribution that is solely defined based on m and ℓ. This allows us to tune the parameters m and ℓ to provide strong guarantees for the coverage $R < R_\ell$ where R_ℓ is obtained from our fixed sampled dataset.

This guarantee can be equivalently expressed as a two-sided probabilistic bound. Specifically, let $\mathsf{betacdf}_\delta(\ell, m+1-\ell)$ denote the cumulative distribution function (CDF) of the Beta distributionalso known as the regularized incomplete beta functionevaluated at δ. Then, based on the definition of cumulative density function, CDF, for any confidence $\delta_1 \in [0, 1]$ and any arbitrary distribution $R \sim \mathcal{D}$, the following inequality holds:

$$\Pr\left[\ \Pr[\ R \leq R_\ell\ ] > \delta_1\ \right] > 1 - \mathsf{betacdf}_{\delta_1}(\ell, m+1-\ell).$$

Note that the key assumption is that all variables $R, R_1, R_2, \ldots, R_m$ are independently drawn from the same distribution $\mathcal{D}$, and that the previously sampled values are sorted such that $R_1 < R_2 < \ldots < R_m$. Importantly, the resulting probabilistic guarantee remains valid for any arbitrary choice of sample size m, rank ℓ, and confidence level δ_1, provided they lie within appropriate bounds.

Appendix B. A Clarifying Example for Conformal Inference

Assume an arbitrary distribution $R \sim \mathcal{D}$. We sample a calibration dataset of size $m = 100,000$, we sort the samples as $R_1 < R_2 < \ldots < R_{100,000}$ and we select the sample at rank $\ell = 99,999$. In this case, given an unseen draw R^{unseen} from $\mathcal{D}$ for a miscoverage level $\epsilon = 0.0001$, the $\langle \epsilon, \ell, m \rangle$ guarantee for logical statement $P(\ell, m) = [R^{\text{unseen}} < R_\ell]$ is:

$$\Pr\left[\ \Pr[\ R^{\text{unseen}} < R_{99,999}\ ] > 0.9999\ \right] > 0.9995008$$

which is valid for any calibration dataset $\mathbf{M} = \{R_1, R_2, \ldots, R_{100,000}\}$ sampled from distribution $\mathcal{D}$ if and only if R^{unseen} is also sampled from $\mathcal{D}$, and $R_{99,999}$ is the $99,999^{\text{th}}$ smallest member of $\mathbf{M}$.

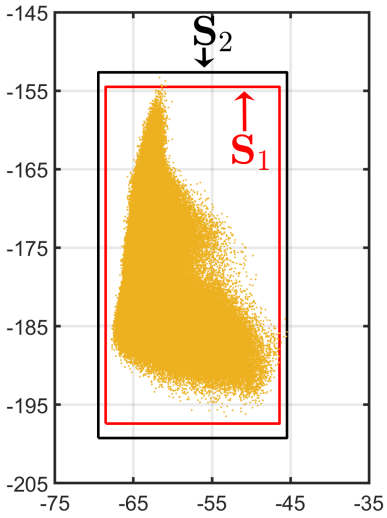

Figure 3: The figure depicts two reachable sets corresponding to different $\langle \epsilon, \ell, m \rangle$ guarantees. Both S_1 and S_2 are obtained using the naïve approach, with S_2 providing a stronger guarantee than S_1.

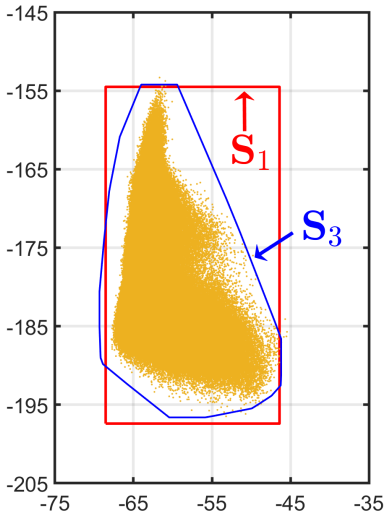

Figure 4: The figure compares two reachable sets with the same $\langle \epsilon, \ell, m \rangle$ guarantees. S_1 is obtained using the naïve approach, while S_3 is produced by the surrogate-based technique, illustrating the accuracy of the latter.

Appendix C. A Clarifying Example on Naive Approach

Since the naive technique is architecture-agnostic we apply that for the reachability analysis of a feedforward ReLU neural network with 60 hidden-layers of width 100, an input layer of dimension 784 and an output layer of dimension 2. The set of inputs is $\mathbf{I} := [0, 1]^{784}$ and we generate both calibration and train datasets by sampling $\mathbf{I}$ uniformly. e.g., $\mathcal{W}, \mathcal{W}'$ are both uniform distributions.

1: We firstly generate a calibration dataset of size $m = 200,000$ and a train dataset of size $t = 10,000$, we also consider the rank $\ell = 199,998$ and we target the miscoverage level of $\epsilon = 0.0001$. In this case we compute a reachable set, $\mathbf{S}_1$ with the following $\langle \epsilon, \ell, m \rangle$ guarantee.

$$x \overset{\mathcal{W}}{\sim} \mathbf{I} \quad \Rightarrow \quad \Pr\left[\ \Pr[\ f(x) \in \mathbf{S}_1 \ ] > 0.9999 \ \right] > 0.9999995. \tag{12}$$

2: Secondly, we set $m = 8464287$, $\ell = 8464286$ and $\epsilon = 0.000002$ which results in another reachset $\mathbf{S}_2$ with the following $\langle \epsilon, \ell, m \rangle$ guarantee.

$$x \overset{\mathcal{W}}{\sim} \mathbf{I} \quad \Rightarrow \quad \Pr\left[\ \Pr[\ f(x) \in \mathbf{S}_2 \ ] > 0.999998 \ \right] > 0.9999992. \tag{13}$$

Figure 3 shows the reachable sets $\mathbf{S}_1$ and $\mathbf{S}_2$ in the presence of 10^6 new simulations, $f(x), x \overset{\mathcal{W}}{\sim} \mathbf{I}$, for validation. Our calculations show that the proportion of points lying outside of $\mathbf{S}_1$ and $\mathbf{S}_2$ are 0.000013 and 0.000001, respectively, which aligns well with the proposed $\langle \epsilon, \ell, m \rangle$ guarantees.

Remark 1 *One might argue that the dimensionality issue can be addressed by partitioning the output layer and performing reachability analysis on each partition separately. However, this approach is suboptimal, as the overall probabilistic guarantee deteriorates. Specifically,*

the combined guarantee is governed by a union bound over the individual partitions, which can lead to an unacceptably loose $\langle \epsilon, \ell, m \rangle$ guarantee.

Appendix D. More Details on Clipping Block, Surrogate Model & Minkowski Sum

The clipping block is the core component of our surrogate model, providing both an accurate approximation of the original system and a deterministic reachable set. Specifically, we first generate a cloud of outputs from the training dataset and construct a convex hull enclosing these points. We formulate this convex hull as,

$$\mathbf{CH} = \sum_{j=1}^{t} \alpha_j \mathbf{vec}(y_j^{\text{train}}), \qquad \mathbf{s.t.} \quad \sum_{j=1}^{t} \alpha_j = 1, \quad \alpha_1, \cdots, \alpha_t > 0$$

The clipping block then applies a convex optimization procedure that projects every unseen output $\mathbf{vec}(y^{\text{unseen}})$ onto this hull, as $\mathbf{vec}(\hat{y}^{\text{unseen}}) = \sum_{j=1}^{t} \alpha_j^* \mathbf{vec}(y_j^{\text{train}})$, where,

$$\alpha_1^*, \cdots, \alpha_t^* = \underset{\alpha_1, \cdots, \alpha_t}{\mathbf{argmin}} \|\mathbf{vec}(y^{\text{unseen}}) - \sum_{j=1}^{t} \alpha_j \mathbf{vec}(y_j^{\text{train}})\|_l \quad \mathbf{s.t.} \ \sum_{j=1}^{t} \alpha_j = 1, \quad \alpha_1, \cdots, \alpha_t > 0,$$

that for $l = 2$ is a quadratic programming and for $l = 1, \infty$ is a linear programming. Among the three options, we are most interested in $l = \infty$, since it minimizes the maximum error across the logit components, making it a suitable choice for reachability analysis. In addition, the $l = 2$ formulation is far more memory-intensive compared to the $l = \infty$ case. When we ran it on the OCTA-500 dataset using the Vortex machine (540 GB RAM), it resulted in an out-of-memory error. We also attempted the PGD variant of quadratic programming for $l = 2$; however, this led to severe CPU thread oversubscription issues. Thus, the LP formulation scales more gracefully. Each problem is linear, and batching helps amortize model builds, and parallelism is also effective which is why we observe it running stably on our setup.

Thus, our surrogate model g is composed of two main components. The first is the base model f, which takes the vectorized image $\mathbf{vec}(x^{\text{unseen}})$ and produces the corresponding logit vector $\mathbf{vec}(y^{\text{unseen}})$. The second is the clipping block, which takes $\mathbf{vec}(y^{\text{unseen}})$ as input and returns its projection onto the convex hull $\mathbf{CH}$, denoted as $\mathbf{vec}(\hat{y}^{\text{unseen}})$. In other words,

$$g(\mathbf{vec}(x^{\text{unseen}})) = \mathbf{vec}(\hat{y}^{\text{unseen}})$$

and obviously $\mathbf{CH}$ represents the deterministic reachable set of the surrogate model, $\mathbf{R}_g(\mathbf{I}) = \mathbf{CH}$.

To generate the convex hull, it is not necessary to include the entire training dataset. Instead, one can identify the extreme points Sartipizadeh and Vincent (2016) and construct the convex hull using only those points, which reduces the number of coefficients α without sacrificing accuracy. This approach makes the convex hull more efficient to be used as it reduces the number of coefficients α. Existing algorithms for identifying extreme points include Quickhull Barber et al. (1996) and Clarksons algorithm Clarkson (1988). Their computational complexities are $\mathcal{O}(t \log(t))$ for $n = 2, 3$ and $\mathcal{O}(t^{\lfloor n/2 \rfloor})$ for $n \geq 4$, which

do not scale well to high-dimensional spaces. Another approach to this problem is to approximate the convex hull by allowing a controlled level of inaccuracy Sartipizadeh and Vincent (2016); Jia et al. (2022). However, as reported in the literature Casadio et al. (2025), this method has not shown promising performance even in high-dimensional settings such as large language models, whose dimensionality is still lower than that of semantic segmentation networks.

For this reason, we keep the original formulation and retain all points in the training dataset when constructing the convex hull. Importantly, this does not create scalability issues for our experiments, since conformal inference is highly data-efficient. For example, guarantees of order $\delta_1 = 0.999$ and $\delta_2 = 0.997$ can be verified with a calibration dataset of size $m = 8000$. Because we consider the size of the training dataset to be at most 50% of the calibration dataset size, then $t = 4000$ training samples suffice for our experiments, requiring only 4000 coefficients α in the convex hull formulation. Moreover, since the number of extreme points grows exponentially with the dimension of the logits, i.e., $\mathcal{O}((\log t)^{n-1})$ Dwyer (1988), it is highly likely that most training samples will serve as extreme points. This renders attempts to distinguish between extreme and interior points largely ineffective.

We employ quadratic (QP) and linear (LP) programming to project unseen points $\mathbf{vec}(y^{\text{unseen}})$ onto the convex hull. However, these optimizations become computationally expensive in high-dimensional settings. To mitigate this, we first apply the learning-based PCA technique in Algorithm 1 to train the matrix of top-N principal directions A, which reduces the dimensionality of logits $\mathbf{vec}(y)$ by computing $v = A^\top \mathbf{vec}(y)$. We then construct the convex hull over the reduced representations $v_j^{\text{train}} = A^\top \mathbf{vec}(y_j^{\text{train}}), j = 1, \cdots, t$, which is subsequently used for clipping to project the unseen vectors v into the convex hull. Thus, denoting the clipping block with **CLP** we can represent the surrogate model for an unseen image x^{unseen} as: $g(\mathbf{vec}(x^{\text{unseen}})) = A\ \mathbf{CLP}(A^\top f(\mathbf{vec}(x^{\text{unseen}})))$.

In addition, we leverage conformal inference to generate a hyper-rectangle that bounds the error $q(\mathbf{vec}(x)) = f(\mathbf{vec}(x)) - g(\mathbf{vec}(x))$ between the models $f(\mathbf{vec}(x))$ and $g(\mathbf{vec}(x))$ with provable guarantees. This hyper-rectangle is then used to inflate the convex hull and obtain the probabilistic reachset. Here, we formulate this inflating hyper-rectangle as a convex hull:

$$\mathbf{HR} = \mathcal{R}_q^\epsilon(\mathcal{W};\ \ell, m) = c + \sum_{i=1}^{n} \beta_i \sigma_i e_i, \qquad \mathbf{s.t.} \quad \sum_{i=1}^{n} \beta_i = 1, \quad \beta_1, \cdots, \beta_n > 0$$

where $e_i \in \mathbb{R}^n$ is the i-th Cartesian unit vector in Euclidean space, σ_i is the magnitude obtained from conformal inference (see Eq. (10)) along direction e_i and c is the center of the hyper-rectangle.

Given this formulation, we compute the Minkowski sum between the deterministic reach set of the surrogate model g and the inflating hyper-rectangle as:

$$\mathcal{R}_f^\epsilon(\mathcal{W}; \ell, m) = \mathcal{R}_g(\mathbf{I}) \oplus \mathcal{R}_q^\epsilon(\mathcal{W};\ \ell, m) = \mathbf{CH} \oplus \mathbf{HR} = c + \sum_{j=1}^{t} \alpha_j A\ v_j^{\text{train}} + \sum_{i=1}^{n} \beta_i \sigma_i e_i,$$

$$\text{where,} \qquad \alpha_1, \cdots, \alpha_t, \beta_1, \cdots, \beta_n \geq 0, \quad \sum_{j=1}^{t} \alpha_j = 1, \quad \sum_{i=1}^{n} \beta_i = 1.$$

Table 2: This table reports the bound ratio, bound_ratio, and the empirical miscoverage level of our reachset, $\hat{\epsilon}$ for a selection of test images, perturbation level and perturbation dimensions. We performed 10^6 inferences to estimate the conservatism. Observing a nonzero $\hat{\epsilon}$ is a promising indication of a low level of conservatism.

Dataset	Model	Image name	# Perturbed Pixels	e	bound_ratio	$\hat{\epsilon}$
Camvid	BiSeNet	0001TP_008790.png	41471×3	5/255	0.5328	3.08e-6

The projection of the probabilistic reach set $\mathcal{R}_f^{\epsilon}(\mathcal{W}; \ell, m)$ onto each class of a given pixel can be performed efficiently. To this end, we collect the training points $v_j^{\text{train}}, ; j = 1, \ldots, t$. Since the mapping from latent space to the original space is linear ($\mathbf{vec}(\hat{y}) = Av$), the vertices of the convex hull in latent space are preserved under this transformation. In other words, if v^* is an extreme point of the convex hull in latent space, then Av^* is an extreme point of the convex hull in the original space. Therefore, we collect the points $\mathbf{vec}(\hat{y}_j^{\text{train}}) = Av_j^{\text{train}}$ and compare them to determine the upper bound $\mathbf{ub}$ and lower bound $\mathbf{lb}$ of the surrogate models predictions. Consequently, the clipping block in the surrogate model ensures that every unseen point $\mathbf{vec}(\hat{y}^{\text{unseen}})$ satisfies

$$\mathbf{lb} \leq \mathbf{vec}(\hat{y}^{\text{unseen}}) < \mathbf{ub}.$$

For a given pixel and class, let the corresponding logit value be the k-th component of $\mathbf{vec}(y^{\text{unseen}})$. Then the projection of the reachset on this component satisfies

$$c(k) + \mathbf{lb}(k) - \sigma_k \leq \mathbf{vec}(y^{\text{unseen}})(k) \leq c(k) + \mathbf{ub}(k) + \sigma_k.$$

We conclude this section with a comparison against our naïve approach. Specifically, we consider the experiment described in Appendix C for the given guarantee in Eq. (12), using a calibration dataset of size $m = 200{,}000$ and compare the resulting bounds. For this comparison, we employ a clipping block that projects with $l = \infty$. We constructed the convex hull using a training dataset of size $t = 4000$. In addition, we sampled a separate dataset of size $t' = 10000$ to compute the normalization factors (see Eq. (8)) prior to performing conformal inference for obtaining the inflating hyper-rectangle. The resulting reachable set, together with the outcome of the naïve approach, in the presence of 10^6 new simulations, $f(x), x \overset{\mathcal{W}}{\sim} \mathbf{I}$, are shown in Figure 4. Our calculation shows the proportion of the points lying outside of the reachset is only 0.000012, which aligns well with the proposed $\langle \epsilon, \ell, m \rangle$ guarantee in Eq. (12).

Appendix E. Additional Research Questions

RQ2: Do State-of-the-Art Deterministic Verification Techniques Scale to the Level Achieved by Our Method on Complex and High-Dimensional SSN Models? We applied techniques such as α-β-CROWN (Zhou et al., 2024) and NNV (Tran et al., 2021) to our segmentation experiments using the UNet1, UNet2, and BiSeNet models in RQ1. However, due to the size of these models and the high perturbation levels considered, both methods encountered out-of-memory errors and failed to complete verification on the same hardware used for our approach. This highlights that while deterministic guarantees are often preferable, they may not always be computationally practical. In such cases, our probabilistic verification method for SSNs offers a scalable and effective alternative.

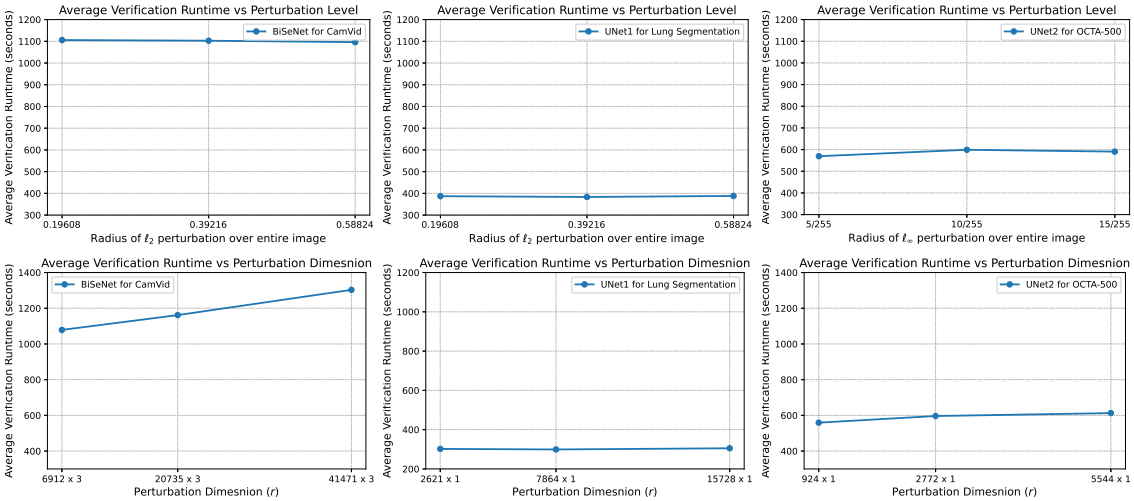

Figure 5: Shows the average run time versus perturbation level (top row) and perturbation dimension r (bottom row). In the top row, the image is entirely perturbed within an ℓ_2 ball for CamVid and Lung Segmentation and ℓ_∞ ball for OCTA-500. In the bottom row, we have darkening adversary where e is fixed at 5/255 across all experiments. The runtimes are averaged over 200 test images from datasets.

RQ3: How Does the Performance of our Methodology Compare to Existing Probabilistic Verification Methods for Neural Networks in the Literature? In this section, we present a comparison with the works of Fiacchini and Alamo (2021); Anani et al. (2024) on the Cityscapes dataset Cordts et al. (2016). Since the formulation of verification guarantees differs slightly across these approaches, we first provide a general overview of the techniques proposed in Fiacchini and Alamo (2021); Anani et al. (2024), followed by a brief description of our own method. This will clarify how the comparison can be meaningfully established.

Overview 1. In Fischer et al. (2021), the authors introduced a probabilistic method to verify Semantic Segmentation Neural Networks. Inspired by Cohen et al. (2019), they introduced randomness via a Gaussian noise $\nu \sim \mathcal{N}(0, \sigma^2) \in \mathbb{R}^{h \times w \times nc}$, applied to the input, and constructed a smoothed version of the segmentation model, denoted $\overline{\mathsf{SSN}}(x)(i,j)$, for each mask pixel (i,j):

$$\overline{\mathsf{SSN}}(x)(i,j) = c_A(i,j) = \arg\max_{c \in \mathbf{L}} \Pr_{\nu \sim \mathcal{N}(0,\sigma^2)} [\mathsf{SSN}(x+\nu)(i,j) = c]$$

They then established that, with confidence level δ_2, the smoothed prediction $\overline{\mathsf{SSN}}(x)(i,j)$ is robust within an ℓ_2 ball $\mathbf{B}_{\bar{r}_{i,j}}(x)$ of radius $\bar{r}_{i,j} = \sigma \Phi^{-1}(\underline{p_A}(i,j))$, where $\underline{p_A}(i,j)$ is a lower bound on the class probability: $p_A(i,j) = \Pr_{\nu \sim \mathcal{N}(0,\sigma^2)} [\overline{\mathsf{SSN}}(x+\nu)(i,j) = c_A(i,j)]$. Here, $\Phi^{-1}(.)$ is the inverse CDF of normal distribution. The corresponding probabilistic guarantee becomes:

$$\forall x' \in \mathbf{B}_{\bar{r}_{i,j}}(x) : \Pr \left[\overline{\mathsf{SSN}}(x')(i,j) = c_A(i,j) \right] \geq \delta_2$$

However, certifying all mask pixels simultaneously is challenging. To enable global guarantees, a more conservative definition of smoothing is adopted: a fixed threshold $\tau \in [0.5, 1]$ is used for all mask locations (i,j) which implies:

(a) Image, 0001TP_008790.png

(b) Predicted Mask from BiSeNet

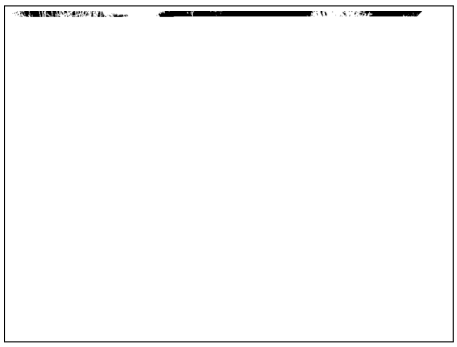

(c) Image perturbed over 6912 darkened pixels.

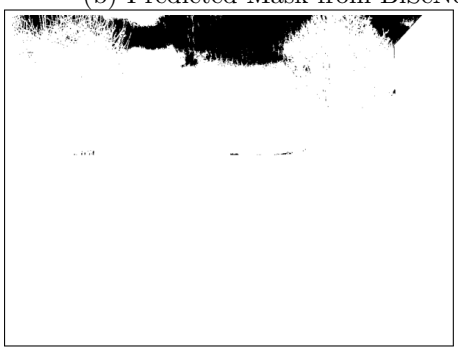

(d) Image perturbed over 41472 darkened pixels.

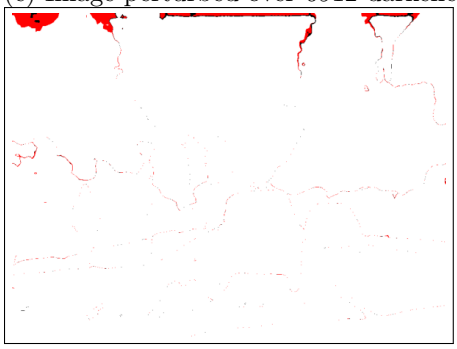

(e) Unknown and non-robust masks for darkening adversary with $e = 5/255$ and $r = 6192 \times 3$.

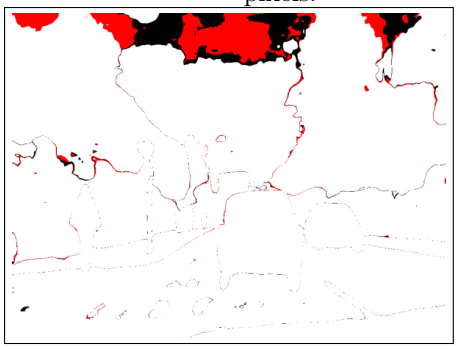

(f) Unknown and non-robust masks for darkening adversary with $e = 5/255$ and $r = 41472 \times 3$.

Figure 6: Visualization for verification on BiSeNet for a test image from the CamVid dataset. (a) Test image. (b) Segmentation mask predicted by BiSeNet. (c,d) Pixels selected for perturbation (in black) on the test image (we sampled 6192 (1%) and 41472 (6%) pixels with R, G, B intensities above 150/255). (e,f) Robust (white), non-robust (red), and unknown (black) pixels for perturbation magnitudes $e = 5/255$ and dimensions $r = 6192 \times 3$ and $r = 41472 \times 3$.

(a) Image, CHNCXR_0005_0.png

(b) Predicted Mask from UNet1

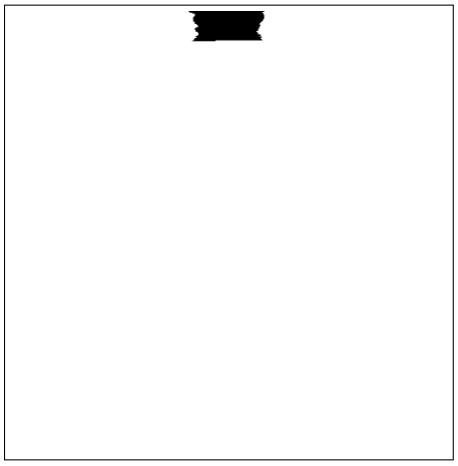

(c) Image perturbed over 2621 darkened pixels.

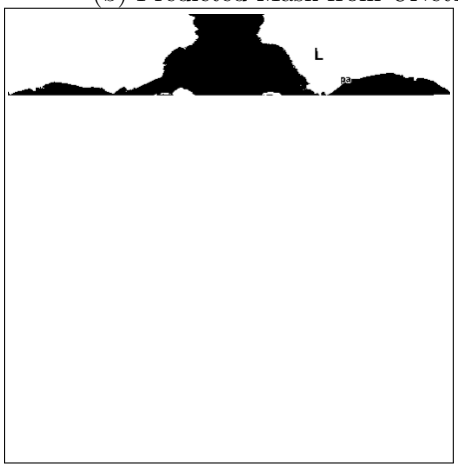

(d) Image perturbed over 15726 darkened pixels.

(e) Unknown and non-robust masks for darkening adversary with $e = 5/255$ and $r = 2621 \times 1$.

(f) Unknown and non-robust masks for darkening adversary with $e = 5/255$ and $r = 15726 \times 1$.

Figure 7: Visualization for verification on UNet1 for a test image from the Lung Segmentation dataset. (a) Test image. (b) Segmentation mask predicted by UNet1. (c,d) Pixels selected for perturbation (in black) on the test image (we sampled 2621 (1%) and 15726 (6%) pixels with Gray intensities above 150/255). (e,f) Robust (white), non-robust (red), and unknown (black) pixels for perturbation magnitudes $e = 5/255$ and dimensions $r = 2621 \times 1$ and $r = 15726 \times 1$.

(a) Image, 10491.bmp from OCTA-500 dataset.

(b) Predicted Mask from UNet2

(c) Image perturbed over 924 darkened pixels.

(d) Image perturbed over 5544 darkened pixels.

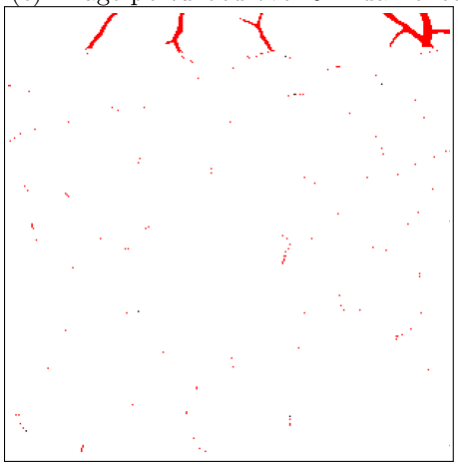

(e) Unknown and non-robust masks for darkening adversary with $e = 5/255$ and $r = 924 \times 1$.

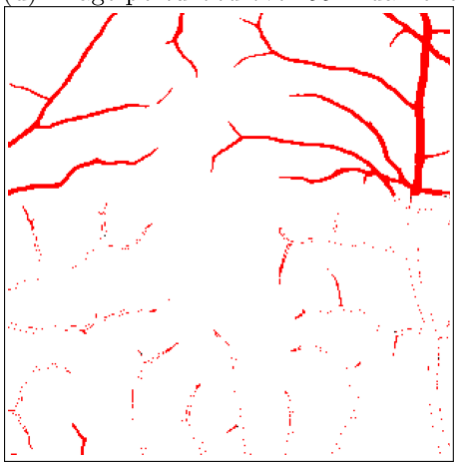

(f) Unknown and non-robust masks for darkening adversary with $e = 5/255$ and $r = 5544 \times 1$.

Figure 8: Visualization for verification on UNet2 for a test image from the OCTA-500 dataset. (a) Test image. (b) Segmentation mask predicted by UNet2. (c,d) Pixels selected for perturbation (in black) on the test image (we sampled 924 (1%) and 5544 (6%) pixels with Gray intensities above 150/255). (e,f) Robust (white), non-robust (red), and unknown (black) pixels for perturbation magnitudes $e = 5/255$ and dimensions $r = 924 \times 1$ and $r = 5544 \times 1$.

$$\overline{\mathsf{SSN}}(x)(i,j) = c_A(i,j), \quad \text{where} \quad \Pr_{\nu\sim\mathcal{N}(0,\sigma^2)}[\mathsf{SSN}(x+\nu)(i,j) = c_A(i,j)] \geq \tau$$

This leads to a unified radius $r = \sigma\Phi^{-1}(\tau)$ for the input space. While this simplifies the formulation, it introduces the concept of **abstained** or uncertifiable pixelsthose that cannot meet the desired confidence threshold. To mitigate the issue of multiple comparisons (i.e., union bounds), the authors propose statistical corrections such as the Bonferroni and HolmBonferroni methods CE (1936); Holm (1979). Assuming the set of certifiable pixels is defined as $\mathbf{CERT} = \{(i,j) \mid (i,j) \text{ is certifiable}\}$, they propose the final guarantee in the following form:

$$\forall x' \in \mathbf{B}_r(x) : \Pr\big[\bigwedge_{(i,j)\in\mathbf{CERT}} \mathsf{P}(i,j)\big] \geq \delta_2, \quad \mathsf{P}(i,j) := \big\{\text{"}\overline{\mathsf{SSN}}(x')(i,j) = c_A(i,j)\text{"}\big\}$$

This method is referred to as SEGCERTIFY. A key limitation of this technique is the presence of abstained pixels. The authors in Anani et al. (2024) addressed this by proposing an adaptive approach, ADAPTIVECERTIFY, which reduces the number of uncertifiable pixels. However, the guarantees proposed in Fiacchini and Alamo (2021); Anani et al. (2024) apply only to the smoothed model, not the base model. To express this in terms of the base model, we define the following problem:

Problem 1. For a given image x, noise $\nu \sim \mathcal{N}(0,\sigma^2)$, and a threshold $\tau \in [0.5, 1]$, define $c_A(i,j) \in \mathbf{L}$ such that: $\Pr_{\nu\sim\mathcal{N}(0,\sigma^2)}[\mathsf{SSN}(x+\nu)(i,j) = c_A(i,j)] \geq \tau$. Then for any $x' \in \mathbf{B}_r(x)$ with $r = \sigma\Phi^{-1}(\tau)$ and confidence level δ_2, we want to show the following guarantee, where **CERT** will be also determined through the verification process:

$$\Pr\big[\bigwedge_{(i,j)\in\mathbf{CERT}} \Pr_{\nu\sim\mathcal{N}(0,\sigma^2)}\big[\mathsf{SSN}(x'+\nu)(i,j) = c_A(i,j)\big] \geq \tau\big] \geq \delta_2$$

Overview 2. In our approach, for a given image x and input set $\mathbf{B}_r(x)$, we perform a probabilistic reachability analysis with a $\langle\epsilon,\ell,m\rangle$ guarantee. Due to the presence of conservatism in our reachability technique, some mask pixels are marked as **robust** (i.e., certifiable), while others cover multiple classes and are considered **unknown** or uncertifiable. Let $\mathbf{CONFORMAL\_CERT} = \{(i,j) \mid (i,j) \text{ is certifiable}\}$. Then our verification objective is:

Problem 2. Given an image x, input set $\mathbf{B}_r(x)$, and sampling distribution $x' \overset{\mathcal{W}}{\sim} \mathbf{B}_r(x)$, for coverage level $\delta_1 = 1-\epsilon \in [0,1]$, hyper-parameters ℓ, m and confidence level $\delta_2 = 1 - \mathsf{betacdf}_{\delta_1}(\ell, m+1-\ell)$, we aim to show the following $\langle\epsilon,\ell,m\rangle$ guarantee, where here the set **CONFORMAL_CERT** will be also determined through the verification process:

$$\Pr\big[\Pr\big[\bigwedge_{(i,j)\in\mathbf{CONFORMAL\_CERT}} \mathsf{SSN}(x')(i,j) = \mathsf{SSN}(x)(i,j)\big] \geq \delta_1\big] \geq \delta_2$$

Comparison. The unknown pixels in our method are conceptually equivalent to the abstained pixels in Fiacchini and Alamo (2021); Anani et al. (2024). Thus, given the same input set $\mathbf{B}_r(x)$ where r is provided by Fiacchini and Alamo (2021), the comparison focuses

Table 3: Percentage of uncertifiable pixels under different (σ, τ, r) settings for Fiacchini and Alamo (2021), Anani et al. (2024), and our Naive approach. The verification runtime is 210 seconds for all experiments.

σ	τ	r	Fiacchini and Alamo (2021) (%)	Anani et al. (2024) (%)	Ours (%)
0.25	0.75	0.1686	7	5	0.0642
0.33	0.75	0.2226	14	10	0.0676
0.50	0.75	0.3372	26	15	0.0705
0.25	0.95	0.4112	12	9	0.0727
0.33	0.95	0.5428	22	18	0.0732
0.50	0.95	0.8224	39	28	0.0758

to show which technique results in fewer uncertifiable mask pixels. To this end, we replicate the setup of Table 1 from Anani et al. (2024), using the same HrNetV2 model Wang et al. (2020)trained on the Cityscapes dataset with the HrNetV2-W48 backbone. In this case study, the results of our Naive approach were approximately equivalent to those of the surrogate-based approach. Therefore, we use the Naive technique for comparison, as it is more efficient than the surrogate-based method. We compare the number of uncertifiable pixels produced by our naive approach against the abstained pixels reported in their results. Our findings are summarized in Table 3, which shows the average over 200 test images. We also report our verification runtime for completeness.